

OXIDATION PATHWAYS OF NATURAL DYE HEMATOXYLIN IN AQUEOUS SOLUTION

Romana SOKOLOVÁ^{a1,*}, Ilaria DEGANO^b, Magdaléna HROMADOVÁ^{a2},
Jana BULÍČKOVÁ^{a3}, Miroslav GÁL^{a4} and Michal VALÁŠEK^c

^a J. Heyrovský Institute of Physical Chemistry, Academy of Sciences of the Czech Republic, v.v.i.,
Dolejškova 3, 182 23 Prague, Czech Republic; e-mail: ¹ sokolova@jh-inst.cas.cz,
² hromadom@jh-inst.cas.cz, ³ bulickov@jh-inst.cas.cz, ⁴ gal@jh-inst.cas.cz

^b Department of Chemistry and Industrial Chemistry, University of Pisa,
Via Risorgimento 35, 56100 Pisa, Italy; e-mail: ilariad@cci.unipi.it

^c Institute of Organic Chemistry and Biochemistry, Academy of Sciences of the Czech Republic, v.v.i.,
Flemingovo nám. 2, 166 10 Prague 6, Czech Republic; e-mail: valasek@uochb.cas.cz

Received August 2, 2010

Accepted September 14, 2010

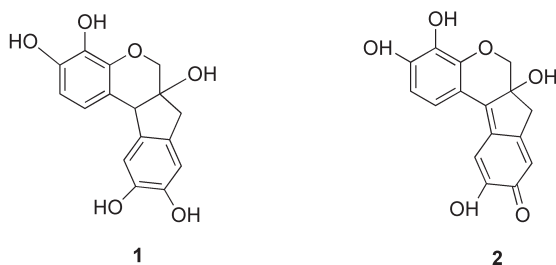
Published online November 9, 2010

The oxidation mechanism of hematoxylin was studied in phosphate buffers and 0.1 M KCl by cyclic voltammetry and UV-Vis spectroscopy under deaerated conditions. The redox potential of hematoxylin in buffered solution strongly depends on pH. A two electron oxidation is preceded by deprotonation. The homogeneous rate of deprotonation process of hematoxylin in 0.1 M phosphate buffer is $k_d = (2.5 \pm 0.1) \times 10^4 \text{ s}^{-1}$. The cyclic voltammetry under unbuffered conditions shows the distribution of various dissociation forms of hematoxylin. The dissociation constants $\text{p}K_1 = 4.7 \pm 0.2$ and $\text{p}K_2 = 9.6 \pm 0.1$ were determined using UV-Vis spectroscopy. The final oxidation product was identified by gas chromatography with mass spectrometry detection as hemathein. The distribution of oxidation products differs under buffered and unbuffered conditions. The dye degradation in natural unbuffered environment yields hemathein and hydroxyhematoxylin, which is absent in buffered solution.

Keywords: Hematoxylin; Oxidation; Dye degradation; Cyclic voltammetry.

Degradation process of flavonoid compounds used as colorants in historical tapestries is a serious problem for the conservation and restoration of the art objects. Hematoxylin 1 and hemathein 2 (Scheme 1) are the principal chromophores of *Hematoxylon campechianum* and *Hematoxylon brasiletto*, two species also known as “logwood”, originating from South America. The original color of medieval textiles is transformed by ambient unbuffered aerobic environment and its color fades away or changes^{1,2}. It is highly desirable to find possible degradation pathways and decomposition products

of the original dyes. Degradation products formed during the aging process can be used as fingerprints for the determination and restoration of the original color.



SCHEME 1

Chemical structures of hematoxylin **1** and hematein **2**

A detailed study of the electrochemical behavior of **1** is missing in the literature, although the electrochemistry and electrocatalytic activity of the hematoxylin-modified carbon paste electrode towards the electrocatalytic oxidation of NADH were reported³. Recently, compound **1** was used as chemical sensor in modified carbon paste electrode, glassy carbon electrode and multi-wall carbon nanotube modified glassy carbon electrode for the determination of some analytes⁴. Hematein **2** was used as a pH-sensitive redox active compound in an amperometric pH-sensing biosensor^{5,6}. The positive shift of anodic peak of cyclic voltammograms of **2** on n-eicosane-graphite composite electrode with decreasing pH was reported⁶. Since compounds **1** and **2** contain the phenolic group it is expected that the oxidation of phenols is relevant for the present study. The anodic oxidation pathways of phenols, polyphenols and hydroquinones have been extensively studied^{7–15}. Their oxidation is generally followed by complicated sequence of coupled chemical reactions. The quinones formed after the oxidation of hydroquinones can undergo the nucleophilic addition of the solvent and a trihydroxyderivative is developed. Its further oxidation causes the formation of hydroxyquinone¹⁶. The influence of pH on electrochemical response of polyphenols and hydroquinones was previously reported^{7,8,11,13}. The aim of this study is the elucidation of oxidative processes in buffered solution of different pH. We will identify the final oxidation products and possibly search for factors, which influence their distribution. Natural degradation of **1** and **2** proceed in an unbuffered environment. Hence, we will look also for effects caused by the absence of buffering medium.

EXPERIMENTAL

Reagents

Hematoxylin **1** was purchased from Fluka. The reagents used as supporting electrolytes such as potassium chloride and chemicals for preparation of phosphate or phosphate/citrate buffers (KH_2PO_4 , NaH_2PO_4 , NaOH , citric acid) were of reagent grade. Phosphate buffers (pH 2.5–12) were prepared at constant ionic strength. The solutions were prepared with ultrapure water (Millipore). All the solvents were Carlo Erba (Milan, Italy) HPLC grade except from ethyl acetate (AcOEt), Anal R, BDH. Hexadecane and 2,4-dihydroxybenzophenone, used as internal standards, and *N,O*-bis(trimethylsilyl)trifluoroacetamide (BSTFA) containing 1% trimethylchlorosilane were purchased from Sigma (Milan, Italy). Stock solutions of analytes in methanol were prepared from **1** from Fluka and **2** (approx. 85%) from Sigma (Milan, Italy). All reagents and chemicals were used without further purification.

Techniques

Electrochemical measurements were done using an electrochemical system for cyclic voltammetry. It consisted of a fast rise-time potentiostat interfaced to a personal computer via an IEEE-interface card (AdvanTech, model PCL-848) and a data acquisition card (PCL-818) using 12-bit precision. Cyclic voltammetry was also conducted using a PGSTAT 12 AUTOLAB potentiostat (Ecochemie, The Netherlands). A three-electrode electrochemical cell was used with an $\text{Ag}|\text{AgCl}|1 \text{ M LiCl}$ reference electrode (with potential 0.210 V vs SHE) separated from the test solution by a salt bridge. The working electrodes were platinum electrode (diameter 0.8 mm) and glassy carbon electrode (diameter 0.7 mm). The auxiliary electrode was cylindrical platinum net. Oxygen was removed from the solution by passing a stream of argon. The oxidation products of **1** were prepared by exhaustive electrolysis of 1.4×10^{-3} – $2.54 \times 10^{-3} \text{ M}$ solutions on a Pt wire or on a carbon paste electrode.

Products were identified using a Trace GC gas chromatograph (Thermo Electron Corporation, USA) equipped with a programmable temperature vaporizing (PTV) injection port and a mass spectrometric detector based on an ion trap analyzer (Polaris Q, Thermo Electron Corporation, USA). The PTV injector was in the CT 'splitless with surge' mode at 280 °C with a surge pressure of 100 kPa, and the mass spectrometer parameters were: electron impact ionization (70 eV), ion source temperature 230 °C, scan range m/z 50–700 and interface temperature 280 °C. Chromatographic separation was performed on a DB-5MS chemically bonded fused silica capillary column (J & W Scientific, Agilent Technologies) with stationary phase 5%phenyl–95%methylpolysiloxane, and of dimensions 0.25 mm i.d., 0.1 µm film thickness, 25 and 30 m length. The gas chromatographic conditions were as follows: initial temperature 57 °C, 2 min isothermal, then ramped at 10 °C/min up to 200 °C, 3 min isothermal, then ramped at 20 °C/min up to 300 °C and then isothermal for 20 min. The carrier gas was He (purity 99.9995%), at a constant flow rate of 1.2 ml/min. The peak assignment was based on comparison with analytical reference compounds and materials, with library mass spectra (NIST 1.7) and with mass spectra reported in the literature.

In order to perform GC-MS analysis, electrolysis products were derivatized with a silylating agent BSTFA. Derivatization conditions were: 10 μl of 2,4-dihydroxybenzophenone (solution in isopropanol, internal standard IS1) were added to the sample, the solution was dried and 30 μl of the derivatization agent BSTFA in 50 μl of AcOEt were added, the reaction took place at 60 $^{\circ}\text{C}$ for 30 min in closed glass vials. Just before injection, 10 μl of hexadecane (solution in isooctane, internal standard IS2) and 150 μl of AcOEt were added, 2 μl of the final solution were injected in the GC system.

A diode-array UV-Vis spectrometer Agilent 8453 with 1.0 cm quartz cuvettes was used for recording of the absorption spectra. The absorption spectra of 1×10^{-5} M hematoxylin in phosphate/citrate buffer in the pH range 2.5 to 11.0 were recorded for 50 s after mixing of solution in the deaerated cell.

RESULTS AND DISCUSSION

Acid-Base Equilibria

The protonation reactions play an important role in the electrochemistry of phenols and quinones. For the elucidation of an overall mechanism it is necessary to determine, which dissociation form is present in the solution at a given pH. The dissociation constants of hematoxylin 1 $\text{p}K_1 = 3.82$ and $\text{p}K_2 = 6.88$ were reported by Masoud et al.¹⁷, who used spectrophotometry. Zare et al.³ published the apparent dissociation constant $\text{p}K' = 8.0$ of 1 incorporated into the carbon paste. The compound 2 has values of $\text{p}K_1 = 6.70$ ¹⁸ and $\text{p}K_2 = 6.86$ ¹⁹ determined by spectrophotometric methods. Since

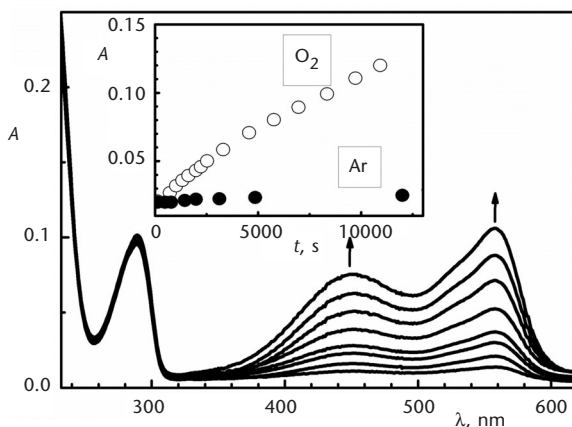


FIG. 1

The change of UV-Vis absorption spectra of 2×10^{-5} M hematoxylin in phosphate buffer at pH 7 under the air oxygen. The inset shows the dependence of absorbance at 560 nm on time under argon atmosphere (●) and under air oxygen (○)

we found strong influence of the air oxygen on the absorption spectra of the compound **1** (Fig. 1), we evaluated the dissociation constants of **1** by recording the absorption spectra in phosphate and phosphate/citrate buffers under strictly deaerated conditions. The absorption spectrum of **1** at pH 2.5 is characterized by the bands with absorption maxima at 237 and 289 nm. The band at 237 nm increases during the change of pH to higher values and slightly undergoes a blue shift. The height of the band at 289 nm does not change. The band with the absorption maximum at 204 nm and a small shoulder at 237 nm occurs in the absorption spectrum of **1** in phosphate buffers at pH higher than 6.5. The band with absorption maximum at 560 nm appears at this pH value and increases with increasing pH until the value of pH 10.4; the band at 204 nm decreases significantly during the same change of pH and the isosbestic point is found at 220 nm. The pH dependence of the maximum absorbance of bands changing due to the acid-base equilibrium is related to pK by the Eq. (1)¹⁸

$$\text{pH} = \text{pK} + \log \frac{A_{\text{max}} - A}{A - A_{\text{min}}} \quad (1)$$

where A_{max} and A_{min} are the maximum and minimum absorbances measured at the maximum and minimum pH values, respectively. The plots of $\log [(A_{\text{max}} - A)/(A - A_{\text{min}})]$ vs pH are linear with the intercept equal to pK and the corresponding slopes ± 1 . The $\text{pK}_1 = 4.7 \pm 0.2$ was estimated from the change of absorption at 232 nm, which was the only change in absorption spectra in acid region recorded in the range of 190 to 700 nm up to pH 7 (Fig. 2a). The limited accuracy of pK_1 estimation is caused by uncertainty in the deconvolution of overlapping absorption bands. The determination of $\text{pK}_2 = 9.6 \pm 0.1$ is considerably more precise. It is obtained from the change of the absorbance at 204 and 560 nm (Fig. 2b), where straight lines have slopes +1 and -1, respectively, and the point of their intersection is well defined. The increase of the absorption band at 560 nm indicates that a dianion of **1** is formed. This band corresponds to a chromophore similar to the anion of the compound **2** reported by Bettinger et al.¹⁸

The absorption band at 289 nm in solution of the compound **1** at pH 9 is accompanied by a shoulder at 305 nm. This shoulder slightly increases with increasing pH. The band at 560 nm shifts to lower wavelength at pH above 10.4. The values of pK_1 and pK_2 were used for comparing the concentration of different dissociation forms of the compound **1** under our experimental conditions. The distribution diagram of various forms is given in Fig. 3. The

undissociated form of hematoxylin 1 is marked as AH_2 , while the first dissociation leads to the anion of 1 AH^- and further dissociation yields dianion of 1 A^{2-} .

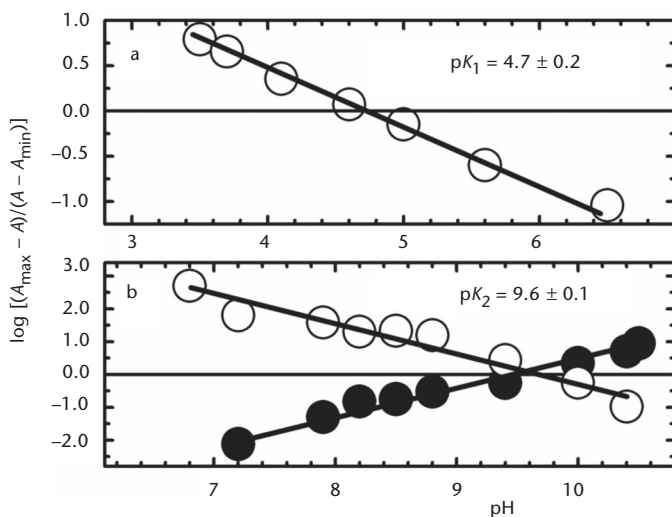


FIG. 2

Plot of $\log [(A_{\max} - A)/(A - A_{\min})]$ versus pH. 1×10^{-5} M hematoxylin in phosphate/citrate buffer (a): 232 (○) nm and in phosphate buffer (b): 204 (●), 560 (○) nm

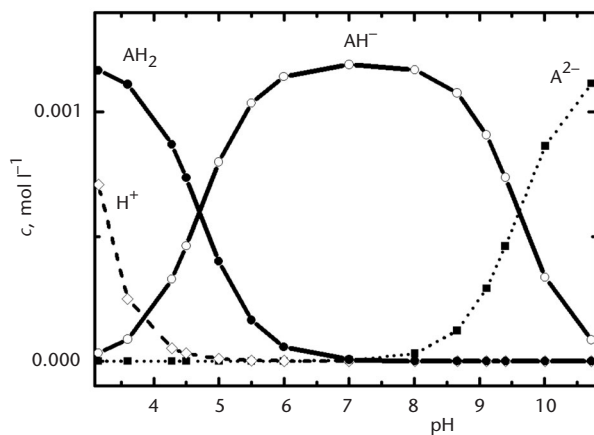


FIG. 3

The distribution of dissociation forms of hematoxylin calculated for total analytical concentration of hematoxylin $1.2 \times 10^{-3} \text{ mol l}^{-1}$

Voltammetry in Buffered Solutions

Cyclic voltammetry of the compound **1** in acidic solution shows one quasi-reversible two-electron oxidation wave and a corresponding cathodic wave (Fig. 4). As the pH of the solution increases, the peak potential of anodic wave is shifted to less positive values and at highest pH the oxidation wave splits into two overlapping peaks. A complete loss of reversibility occurs at $\text{pH} > 6.9$, indicating that under these conditions the primarily generated product is not stable. The concentration of **1** does not have an influence on the potential of the anodic peak. This proves an absence of a bimolecular chemical process. The increase of the anodic peak current with the increasing pH is given in the inset of Fig. 4. The peak currents of **1** in the phosphate buffer at pH 4.9 (curve 1 in Fig. 4) are linearly dependent on the square root of the scan rate. A similar linear dependence on the square root of the scan rate in the range of 0.005 to 1 V s^{-1} holds for all pH values. Thus the oxidation process is diffusion controlled over the whole pH range. The anodic peak potential shifts towards more positive values with an increase of the scan rate by 20 mV per decade. From these observations one can conclude that an acidobasic equilibrium participates significantly in the mechanism of oxidation²⁰

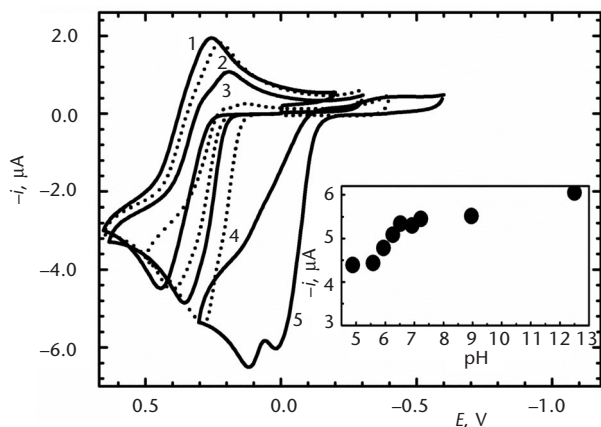
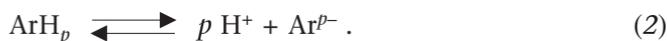


FIG. 4

Cyclic voltammogram of 1.2×10^{-3} M hematoxylin in phosphate buffer on Pt microelectrode at pH 4.9 (1), 5.6 (2), 5.9 (3), 6.9 (4) and 12.5 (5) and at the scan rate of 0.05 V s^{-1} . Cyclic voltammograms of pH 6.3, 6.5 and 7.2 are not shown. The dependence of the anodic peak current on pH is shown in the inset

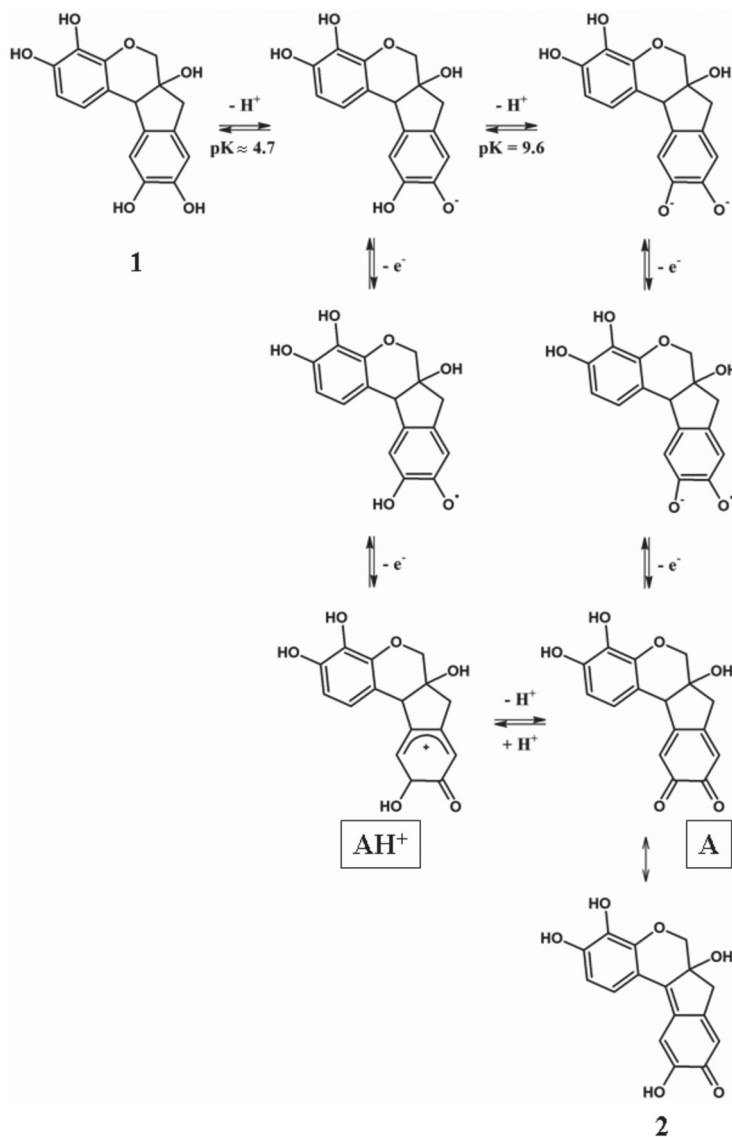
Here ArH_p denotes the natural form of the studied organic molecule and p is the number of protons participating in the overall mechanism. Voltammetric results indicate that the electroactive form is Ar^{p-} , which is formed by the dissociation of proton from the phenolic group. The presence of proton participation in the overall chemical reaction is supported by the shift of anodic peak potential towards lower values. The number of hydrogen ions p , participating in the chemical reaction preceding to the electron transfer, can be estimated from the dependence of the half-wave potential $E_{1/2}$ on the pH of the solution²¹

$$\frac{\partial E_{1/2}}{\partial \ln[\text{H}^+]} = p \frac{RT}{\alpha nF} \quad (3)$$

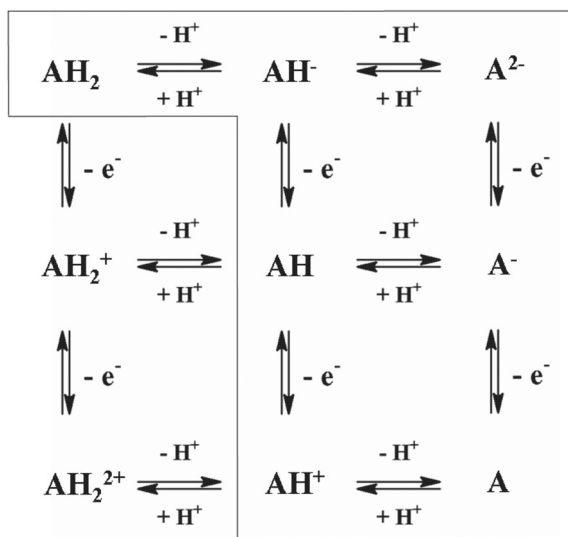
where n is number of electrons involved in the electron transfer. The log-plot analysis of semi-integrated currents yields a slope 95 mV per decade, which is independent on pH. This indicates that the rate of the heterogeneous electron transfer is pH independent. The pH dependence of the half-wave potential of semiintegrated currents gives two linear segments with slopes 92 mV pH^{-1} and 28 mV pH^{-1} . The two lines intersect at the point, which corresponds to the apparent dissociation constant $\text{p}K_2' = 6.7$ (not shown). The observed slope $2.3RT/\alpha nF = 95$ mV and the estimated slope of the dependence of half-wave potential on the concentration of H^+ according to Eq. (3) is equal to 92 mV pH^{-1} . This yields the number of dissociated protons $p = 0.97$. Therefore for pH lower than $\text{p}K_1$, only one hydrogen ion participates in the rate-determining preceding deprotonation (Scheme 2). This scheme resembles the 'schema carre'²² (Scheme 3) and the mechanism in buffered solution proceeds through the formation of a monoanion and the acceptance of two electrons. The mechanism involves the formation of phenoxy cation^{8,16} and the compound **2** is the final product. Therefore, the electroactive form responsible for the main oxidation wave is an anionic form of the compound **1**.

The inset in Fig. 4 shows that the oxidation currents at $\text{pH} < 7$ decrease with the decreasing pH. The oxidation current becomes controlled by the rate of the preceding dissociation, which yields the electroactive monoanion or dianion of **1**. The oxidation currents at $\text{pH} < 7$ and the determined values of K_1 and K_2 enable the estimation of the rate of the homogeneous deprotonation. For this purpose, the voltammograms were numerically transformed by semiintegration to S-shaped waves. The limiting semi-integrated currents yield the k_d rate constant of the preceding dissociation

(Eq. (2)) on the basis of the Koutecký theory²³. The ratio of the semi-integrated limiting kinetic current I_k to the diffusion limited semiintegrated current I_d is related to rate parameters by a tabulated function $F(\chi) = I_k/I_d$.



SCHEME 2
The oxidation of hematoxylin 1



SCHEME 3
The 'schema carre'

The parameter χ is a function of a monomolecular rate constant ρ and a corresponding equilibrium constant of the chemical reaction σ . For the equilibrium Eq. (2) and $p = 1$, the substitution $\rho = k_d \times [\text{AH}]$ and $\sigma = [\text{H}^+]/K$ in the Koutecký equation yields the expression

$$k_d = 0.58 \frac{\chi^2 [\text{H}^+]}{K[\text{AH}]t}. \quad (4)$$

The estimated value of the rate constant of dissociation in 0.1 M phosphate buffer is $k_d = (2.5 \pm 0.1) \times 10^4 \text{ s}^{-1}$ (Fig. 5). The concentration of the supporting electrolyte does not have any influence on the shape of the oxidation waves, which indicates an absence of the double-layer effects.

The exhaustive electrolysis at a constant potential was performed in order to obtain the oxidation products of the compound **1**. We report here the products obtained at two different representative pH values of 5.9 and 9.0. The electric charge required for an exhaustive electrolysis at pH 5.9 corresponds to the consumption of two electrons. The products obtained by an exhaustive electrolysis were separated and GC-MS analysis confirmed the formation of **2** as the main product under buffered conditions. The main peaks in the MS of derivatized hemathein-4TMS correspond to m/z values:

588 ($[M]^{*+}$), 573 ($[M - CH_3]^+$), 560 ($[M - CO]^{*+}$), 545 ($[M - CO - CH_3]^+$), 471 ($[M - CO - OTMS]^+$), 73 ($[TMS]^{*+}$).

The UV-Vis spectrum obtained during the electrolysis (Fig. 6) shows the increase of bands at 292 and 442 nm with slight shoulder at 560 nm, which indicates the formation of the compound 2. The absorption spectra of 2 at the same pH were reported by Bettinger et al.¹⁸, giving $\lambda_{max} = 445$ nm for 2

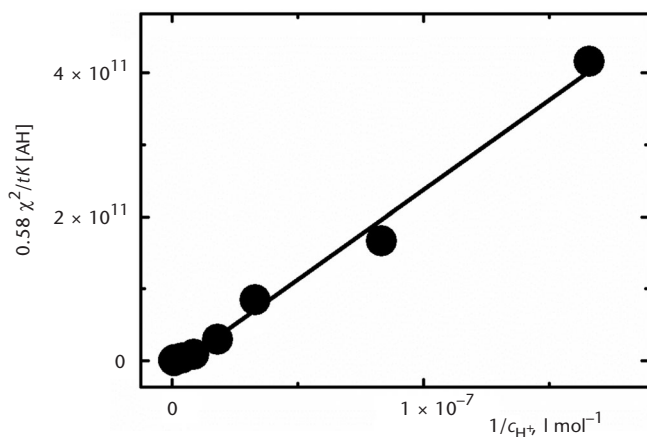


FIG. 5

The plot of $0.58 \chi^2/tK [AH]$ versus $1/[H^+]$ for analytical concentration of hematoxylin $1.2 \times 10^{-3} \text{ mol l}^{-1}$

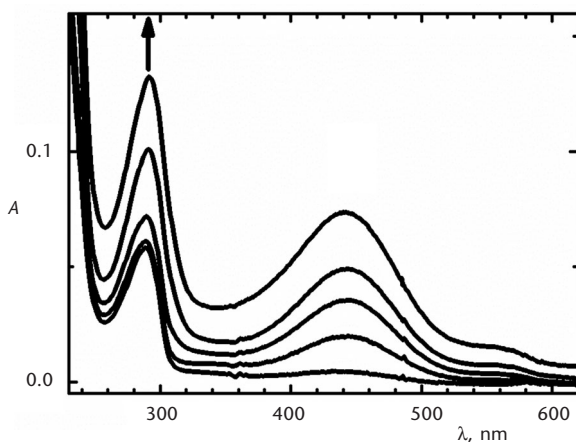


FIG. 6

The change of UV-Vis absorption spectra of $1.1 \times 10^{-5} \text{ M}$ hematoxylin during the exhaustive electrolysis at 0.55 V in phosphate buffer at pH 5.9

and 556 nm for its anion. This behavior is analogous to the oxidation pathway of catechol studied by Petrucci et al.²⁴.

The absorption spectra obtained during the electrolysis of **1** in phosphate buffer at pH 9 (not shown) show sharp increasing absorption band at 560 nm, which is consistent with the formation of **2** (confirmed as the main oxidation product also by GC-MS analysis). The electrolysis in buffered solution at pH 9 proceeded very slowly and did not reach completion. The curve 1 in Fig. 7 shows the absorption spectrum of the solution of **1** after the electrolysis. When the solution was subjected to contact with air further increase of the absorption band at 560 nm was observed. In addition, a new absorption band at 720 nm appears (curve 2 in Fig. 7). These absorption bands completely disappear in 1 h (curve 3 in Fig. 7) due to the following chemical reaction most likely the addition of water. This effect was found by Herath et al.²⁵, who described the complete disappearance of the magenta color in oxidized state within a two hour irradiation in the presence of a photosensitizer. The process dealing with the change of absorption bands (curves 2 and 3 in Fig. 7) does not occur under deaerated conditions.

The strong influence of air oxygen on the absorption spectra of the compound **2** can explain the certain inconsistency in values of p*K* of **1** and **2** reported in literature. The correct values of p*K* of **1** and **2** reported so far

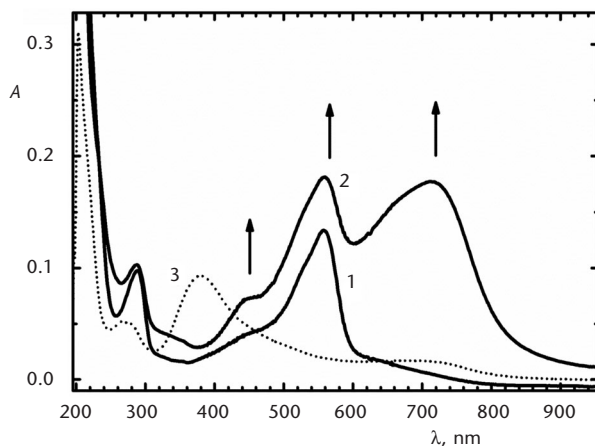


FIG. 7

The absorption spectra of 1.14×10^{-5} M hematoxylin after the exhaustive electrolysis at 0.25 V in phosphate buffer at pH 9 in deaerated cell (1), in the presence of oxygen in 600 s after the opening of the spectrophotometric cell (2) and in the presence of oxygen in 1 h after opening of the spectrophotometric cell (3)

in literature cannot be identified without knowledge of the exact experimental conditions used. This is due to the high unstability of **2** in contact with oxygen, as we demonstrated in Fig. 7.

Voltammetry in Unbuffered Solutions

We recall that the elucidation of a pH dependent decomposition of **1** in buffered media may be different from processes occurring in natural environment without a presence of pH buffering medium. Therefore we will investigate the oxidation in unbuffered media, which is not a standard procedure in organic electrochemistry. Quan et al.²⁶ used with advantage the difference in unbuffered and buffered solution for a complete knowledge of the redox processes of quinones.

In unbuffered solution the cyclic voltammograms have different shapes. The oxidation in the unbuffered solution proceeds at more positive potentials than in buffered solution due to the changes in reaction layer caused by the local change of protons concentration. The main oxidation wave of AH^- anion at 0.52 V decreases at pH higher than 7.0 (Fig. 8). This decrease with the increasing pH is in agreement with the distribution of species in the solution (Fig. 3). The oxidation wave at 0.043 V rises and increases with

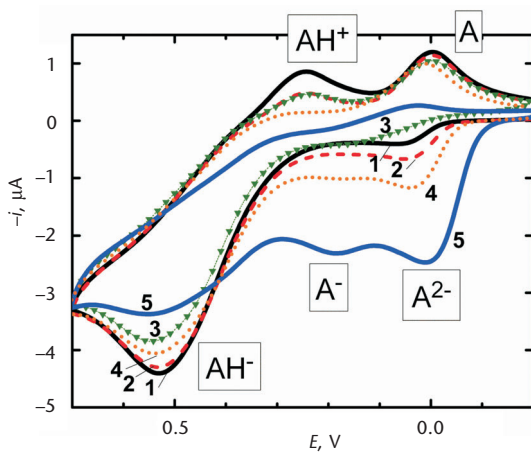


FIG. 8

Cyclic voltammogram of $1.4 \times 10^{-3} \text{ M}$ hematoxylin under unbuffered conditions in 0.1 M KCl on Pt microelectrode at pH 8.0 (1), 8.7 (2), 8.7 (3; second scan), 9.1 (4) and 10.0 (5) at the scan rate of 0.05 V s^{-1} . The pH of solution remained unchanged after the performing of the cyclic voltammogram

the increasing pH. It corresponds to the irreversible oxidation of dianion A^{2-} . There is no cathodic wave when the potential scan is switched at 0.15 V (curve not shown for clarity). At low pH the phenoxycation is formed (see Scheme 2) and gradually becomes the predominant form. This is in agreement with the previous finding that the primarily generated product should be stabilized at pH lower than 6.9. The potential of the oxidation of dianion A^{2-} depends on the apparent pH near the electrode surface because under unbuffered conditions the concentration of H^+/OH^- is not high enough compared to the concentration of the sample¹¹. When the potential scan is reversed at 0.7 V (curve 1 in Fig. 8), a new reduction wave occurs at 0.0 V. This wave is related to the product of the subsequent chemical reactions of phenoxycation AH^+ formed during the oxidation at 0.52 V. The reversible reduction of keto-form of **2** resembles the reported reduction of benzoquinones²⁶. We suggest that it is the reversible reduction of related quinone moiety



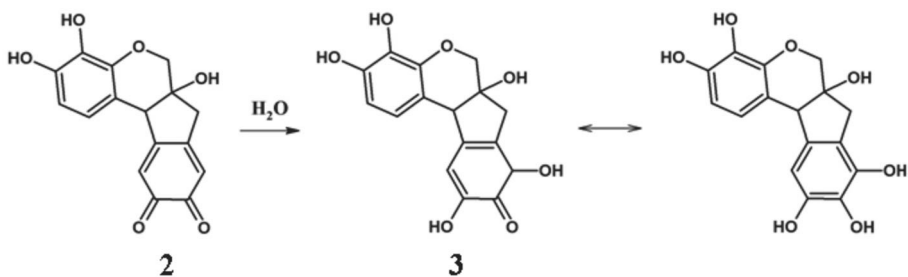
Its oxidation counterpart is visible at the second scan (curve 3 in Fig. 8). Another oxidation wave at 0.185 V appears at $pH > 9$ (curve 4 in Fig. 8). Since the main oxidation wave is the oxidation of AH^- form of **1** and the oxidation of dianion A^{2-} occurs at 0.043 V, the oxidation wave at 0.185 V corresponds to the oxidation of A^- , which is the oxidation product of dianion



The anodic peak potential of this wave agrees with the anodic peak potential of the redox pair A/A^- , which appears during the second scan.

The exhaustive electrolysis at a constant anodic peak potential was performed in order to obtain the oxidation products of **1** also in the unbuffered solution (Fig. 9). The electric charge required for an exhaustive electrolysis at constant anodic peak potentials 0.52 V corresponds to the consumption of two electrons as in the case of buffered solutions. The electrolysis at 0.52 V yields **2** as a main product and several minor products. One of them is hydroxyhematoxylin **3** which can be formed by nucleophilic addition of water to keto-form of **2** (Scheme 4). This was confirmed by the mass spectrum of derivatized hydroxyhematoxylin-5TMS, which yields main peaks at m/z values 678 ($[M]^{*+}$), 663 ($[M - CH_3]^{*+}$), 660 ($[M -$

$\text{H}_2\text{O}]^{*+}$, 645 ($[\text{M} - \text{H}_2\text{O} - \text{CH}_3]^+$), 588 ($[\text{M} - \text{HOTMS}]^{*+}$), 573 ($[\text{M} - \text{CH}_3 - \text{HOTMS}]^+$), 483 ($[\text{M} - \text{CH}_3 - 2 \text{HOTMS}]^+$), 73 ($[\text{TMS}]^{*+}$). Its mass spectrum is consistent with the mass spectrum of derivatized 1: 662 ($[\text{M}]^{*+}$), 647 ($[\text{M} - \text{CH}_3]^+$), 572 ($[\text{M} - \text{HOTMS}]^{*+}$), 557 ($[\text{M} - \text{CH}_3 - \text{HOTMS}]^+$), 483 ($[\text{M} - \text{HOTMS} - \text{OTMS}]^+$), 73 ($[\text{TMS}]^{*+}$). The amount of this product is relatively small (about 7%) due to the fact that in unbuffered solution the pH of solution changes during the electrolysis towards lower values. Under these conditions the enol-form of 2 prevails and the nucleophilic addition of water to keto-form is disfavored. The absorption spectrum of the solution oxi-



SCHEME 4
The formation of hydroxyhematoxylin 3

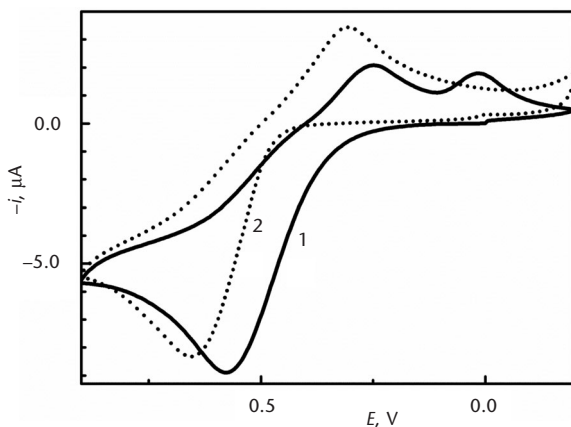


FIG. 9
Cyclic voltammogram of 2.54×10^{-3} M hematoxylin in 0.1 M KCl on Pt microelectrode at the scan rate of 0.05 V s^{-1} before (1) and after (2) electrolysis on Pt wire at 0.52 V

dized at 0.6 V (Fig. 10) shows an increase in the absorption bands at 204, 289 and 440 nm. During the electrolysis a new band is formed, next to the one at 440 nm. The new band at 389 nm indicates that a product of oxidation undergoes further chemical reaction. Similar behavior was mentioned by Papouchado et al.⁷ in the case of catechol in 2 M perchloric acid, where new absorption band matches completely the profile of the oxidized 1,2,4-trihydroxybenzene. The gas chromatogram of electrolyzed **1** at 0.6 V shows two main products at the retention time $t_R = 32.80$ and 33.34 min in 3:1 ratio. This result is in agreement with absorption spectra performed during the electrolysis (Fig. 10) and the absorption band at 389 nm can be due to the presence of compound with shorter retention time. The mass spectrum of this derivatized product (MW 646) has main peaks at m/z values 646, 631, 589, 571 and 483. This oxidation product was not found under buffered conditions. The product with a longer retention time was identified by GC-MS analysis as the compound **2**.

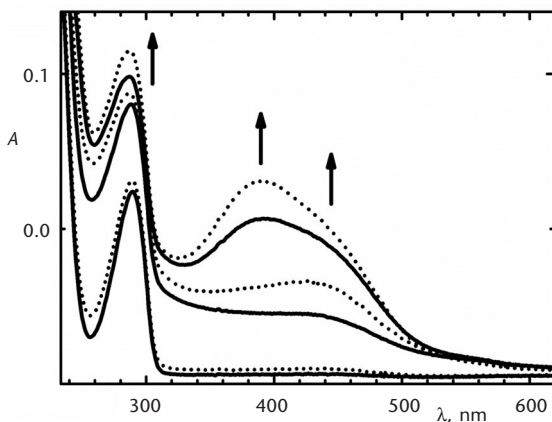


FIG. 10

The change of UV-Vis absorption spectra of 1.1×10^{-5} M hematoxylin during the exhaustive electrolysis at 0.6 V in 0.1 M KCl

CONCLUSIONS

The oxidation mechanism of hematoxylin depends on the pH of solution and its pathway is given by the distribution of various dissociation forms in solution, which can be described using the known scheme 'carré'. We confirmed that a two electron oxidation is preceded by the dissociation of hematoxylin. Hemathein is a product of oxidation in a wide range of pH

from 4.9 to 12. At pH higher than pK_2 , the reaction pathway leads to the formation of a dianion, which is oxidized at lower potentials. We identified that in an unbuffered solution also two redox steps are present, which were clearly distinguished by cyclic voltammetry. They are in agreement with the distribution of species in the solution. Hemathein is formed as the main product also by oxidation of the unbuffered samples. Hydroxyhematoxylin is a minor product, which results from nucleophilic addition of water on keto-form of hemathein. We can conclude that the dye degradation in natural unbuffered environment yields hemathein and hydroxyhematoxylin, which was absent in buffered solution.

This work was supported by the Czech Science Foundation (203/09/1607 and 203/08/1157) and the Ministry of Education, Youth and Sports of the Czech Republic (COST OC140).

REFERENCES

1. Schweppe H.: *Handbuch der Naturfarbstoffe*. Vorkommen, Verlagsgesellschaft. Landeberg/Lech, 1992.
2. Ferreira E. S. B., Quye A., McNab H., Hulme A. N.: *Dyes in History and Archaeology* **2002**, 18, 63.
3. Zare H. R., Nasirizadeh N., Mazloum-Ardakani M., Namazian M.: *Sens. Actuators, B* **2006**, 120, 288.
4. Zare H. R., Nasirizadeh N.: *Sens. Actuators, B* **2010**, 143, 666.
5. Středanský M., Pizzariello A., Středanská S., Miertuš S.: *Anal. Chim. Acta* **2000**, 415, 151.
6. Pizzariello A., Středanský M., Středanská S., Miertuš S.: *Talanta* **2001**, 54, 763.
7. Papouchado L., Petrie G., Adams R. N.: *J. Electroanal. Chem. Interfacial. Electrochem.* **1972**, 38, 389.
8. Nilsson A., Ronlan A., Parker V. D.: *J. Chem. Soc., Perkin Trans. 1* **1973**, 2337.
9. Papouchado L., Sandford R. W., Petrie G., Adams R. N.: *J. Electroanal. Chem. Interfacial. Electrochem.* **1975**, 65, 275.
10. Bailey S. I., Ritchie I. M.: *J. Chem. Soc., Perkin Trans. 2* **1983**, 645.
11. Bailey S. I., Ritchie I. M.: *Electrochim. Acta* **1985**, 30, 3.
12. Hapiot P., Neudeck A., Pinson J., Fulcrand H., Neta P., Rolando Ch.: *J. Electroanal. Chem.* **1996**, 405, 169.
13. Ryan M. D., Yueh A., Chen W.-Y.: *J. Electrochem. Soc.* **1980**, 127, 1489.
14. Hotta H., Sakamoto H., Nagano S., Osakai T., Tsujino Y.: *Biochim. Biophys. Acta* **2001**, 159.
15. Lalor G. C.: *J. Soc. Dyers Colour* **1962**, 78, 549.
16. Morrow G. W.: *Anodic Oxidation of Oxygen-Containing Compounds in Organic Electrochemistry* (H. Lund and O. Hammerich, Eds), 4th ed., p. 589. Marcel Dekker, Inc., New York 2001.
17. Masoud M. S., Hagaag S. S.: *Indian J. Chem., Sect. A: Inorg., Phys., Theor. Anal.* **1982**, 21, 323.
18. Bettinger Ch., Zimmermann H. W.: *Histochemistry* **1991**, 95, 279.

19. Lalor G. C., Martin S. L.: *J. Soc. Dyers Colour* **1959**, 75, 517.
20. Brown E. R., Sandifer J. R. in: *Physical Methods of Chemistry* (B. W. Rossiter and J. F. Hamilton, Eds), Vol. II, pp. 273–314. John Wiley & Sons, Inc., New York 1986.
21. Koryta J.: *Electrochim. Acta* **1959**, 1, 26.
22. Jacq J.: *J. Electroanal. Chem. Interfacial. Electrochem.* **1971**, 29, 149.
23. Koutecký J.: *Collect. Czech. Chem. Commun.* **1953**, 18, 597.
24. Petrucci R., Astolfi P., Greci L., Firuzi O., Saso L., Marrosu G.: *Electrochim. Acta* **2007**, 52, 2461.
25. Herath A., Priyantha N., Rajapakse G., Karunaratne V., Wickramasinghe A.: *J. Natl. Sci. Foundation Sri Lanka* **2007**, 35, 239.
26. Quan M., Sanchez D., Wasylykiv M. F., Smith D. K.: *J. Am. Chem. Soc.* **2007**, 129, 12847.